Article

Cell Reports

Spine Patterning Is Guided by Segmentation of the Notochord Sheath

Graphical Abstract

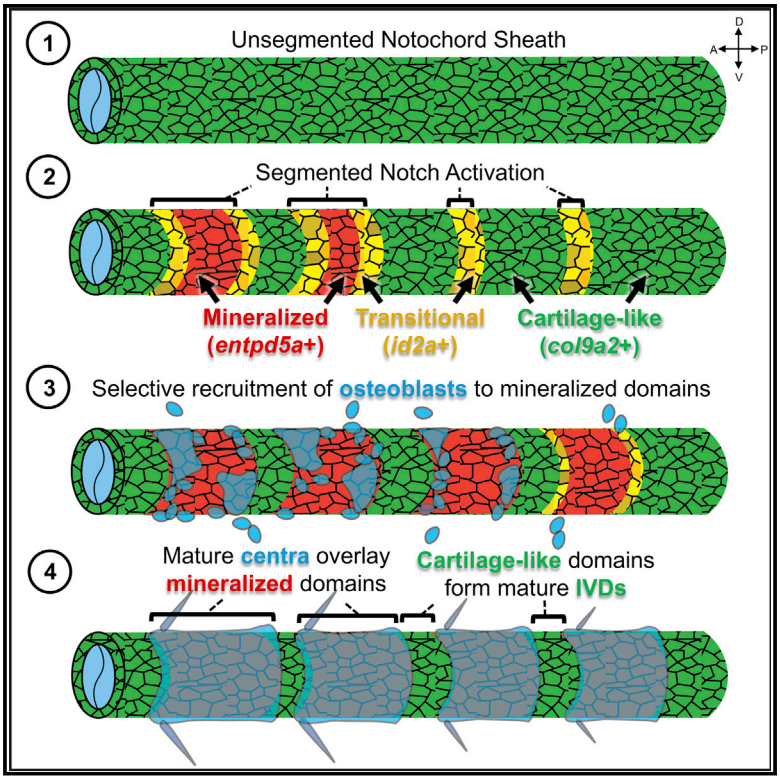

Authors

Susan Wopat, Jennifer Bagwell, Kaelyn D. Sumigray, ..., Kenneth D. Poss, Stefan Schulte-Merker, Michel Bagnat

Correspondence

m.bagnat@cellbio.duke.edu

In Brief

Wopat et al. show that the outer layer of the zebrafish notochord, the sheath, segments into alternating mineralizing and cartilage-like domains prior to vertebral body formation. Mineralized sheath domains, patterned by the segmented activation of Notch, then recruit osteoblasts to form vertebral bodies. Thus, the notochord instructs spine patterning.

Highlights

- The notochord sheath segments into alternating cartilaginous and mineralizing areas
- Segmented activation of Notch patterns the mineralized sheath domains
- Osteoblasts are selectively recruited to mineralized sheath segments
- Notochord sheath segmentation provides a template for spine patterning

Data and Software Availability

GSE109176

Wopat et al., 2018, Cell Reports *22*, 2026–2038
February 20, 2018 © 2018 The Author(s).
https://doi.org/10.1016/j.celrep.2018.01.084

CellPress

OPEN ACCESS
CellPress

Cell Reports
Article

Spine Patterning Is Guided by Segmentation of the Notochord Sheath

Susan Wopat,[1] Jennifer Bagwell,[1] Kaelyn D. Sumigray,[1,2] Amy L. Dickson,[1,6] Leonie F.A. Huitema,[3] Kenneth D. Poss,[1,6] Stefan Schulte-Merker,[3,4,5] and Michel Bagnat[1,6,7,*]

[1]Department of Cell Biology, Duke University Medical Center, Durham, NC 27710, USA
[2]Department of Dermatology, Duke University Medical Center, Durham, NC 27710, USA
[3]Hubrecht Institute – KNAW & UMC Utrecht, 3584 CT, Utrecht, the Netherlands
[4]Institute for Cardiovascular Organogenesis and Regeneration, Faculty of Medicine, WWU Münster, 48149 Münster, Germany
[5]CiM Cluster of Excellence (EXC1003-CiM), 48149 Münster, Germany
[6]Regeneration Next, Duke University, Durham, NC 27710, USA
[7]Lead Contact
*Correspondence: m.bagnat@cellbio.duke.edu
https://doi.org/10.1016/j.celrep.2018.01.084

SUMMARY

The spine is a segmented axial structure made of alternating vertebral bodies (centra) and intervertebral discs (IVDs) assembled around the notochord. Here, we show that, prior to centra formation, the outer epithelial cell layer of the zebrafish notochord, the sheath, segments into alternating domains corresponding to the prospective centra and IVD areas. This process occurs sequentially in an anteroposterior direction via the activation of Notch signaling in alternating segments of the sheath, which transition from cartilaginous to mineralizing domains. Subsequently, osteoblasts are recruited to the mineralized domains of the notochord sheath to form mature centra. Tissue-specific manipulation of Notch signaling in sheath cells produces notochord segmentation defects that are mirrored in the spine. Together, our findings demonstrate that notochord sheath segmentation provides a template for vertebral patterning in the zebrafish spine.

INTRODUCTION

Segmentation of the vertebrate trunk starts during embryogenesis with the formation of somites within the presomitic mesoderm (PSM) (Hubaud and Pourquié, 2014; Pourquié, 2011). This process is controlled in part by the segmentation clock, which acts on the PSM to produce somites in a sequential and highly coordinated fashion (Holley et al., 2002; Oates et al., 2012). Synchronization of the segmentation clock between cells that assemble into discrete somites depends on the Notch pathway, which coordinates gene expression oscillations across cell boundaries (Jiang et al., 2000). The Notch pathway also regulates the period of the segmentation clock and thus also controls somite size and number (Liao et al., 2016). Following somitogenesis, re-segmentation of the paraxial mesoderm (PM) and condensation of the ventral-medial portion, the sclerotome, around the notochord is thought to underlie the generation of discrete vertebral bodies (centra) (Fleming et al., 2015; Renn et al., 2013). The concept of re-segmentation was introduced by Remak in 1855 (Remak, 1855) to explain the spatial mismatch between the segments of the PM and the vertebral bodies of the spine. Since then, this paradigm has been re-visited, validated, and modified in different vertebrate animal models (Bagnall et al., 1988; Ewan and Everett, 1992; Morin-Kensicki et al., 2002; Ward et al., 2017). However, the cellular and molecular processes that underlie the transition from the metameric pattern of the PM to that of the spine remain unknown. Particularly, how sclerotome-derived cells condense around the notochord to produce precise vertebral segments with sharp boundaries separated by regular gaps remains unresolved. Moreover, although mutations in the Notch pathway lead to somite segmentation and to vertebral patterning defects in mice and humans (Sparrow et al., 2012; Turnpenny et al., 2007), it is unclear whether the segmentation machinery acts primarily on the PM, the notochord, or both. Furthermore, it is also unclear if those Notch pathway mutations also affect other cues that may instruct vertebral patterning later in development.

Embryological experiments in chick and zebrafish (Fleming et al., 2004; Haga et al., 2009; Ward et al., 2017; Watterson et al., 1954) and anatomical studies in salmon (Grotmol et al., 2003; Wang et al., 2014) have suggested that the notochord is somehow linked to spine patterning. Furthermore, mouse genetic manipulations have implicated the notochord in spine development (Choi and Harfe, 2011). However, it is not known whether or how the notochord influences the segmentation pattern of the spine. Determining whether the notochord instructs spine patterning will shed light on spine morphogenesis and the origin of vertebral defects.

Here, we use live imaging of transgenic zebrafish, transcriptomic analyses, and tissue-specific genetic manipulations to investigate the role of the notochord in spine patterning. We show that the outer epithelial cell layer of the zebrafish notochord, the sheath, segments into alternating cartilage-like and mineralizing domains prior to the formation of centra. Similar to somitogenesis, notochord sheath segmentation occurs sequentially in an anteroposterior direction. Subsequently, osteoblasts are recruited to the surface of the mineralized sheath domains to form mature vertebral bodies. Gene expression analyses

 © 2018 The Author(s).
This is an open access article under the CC BY-NC-ND license (http://creativecommons.org/licenses/by-nc-nd/4.0/).

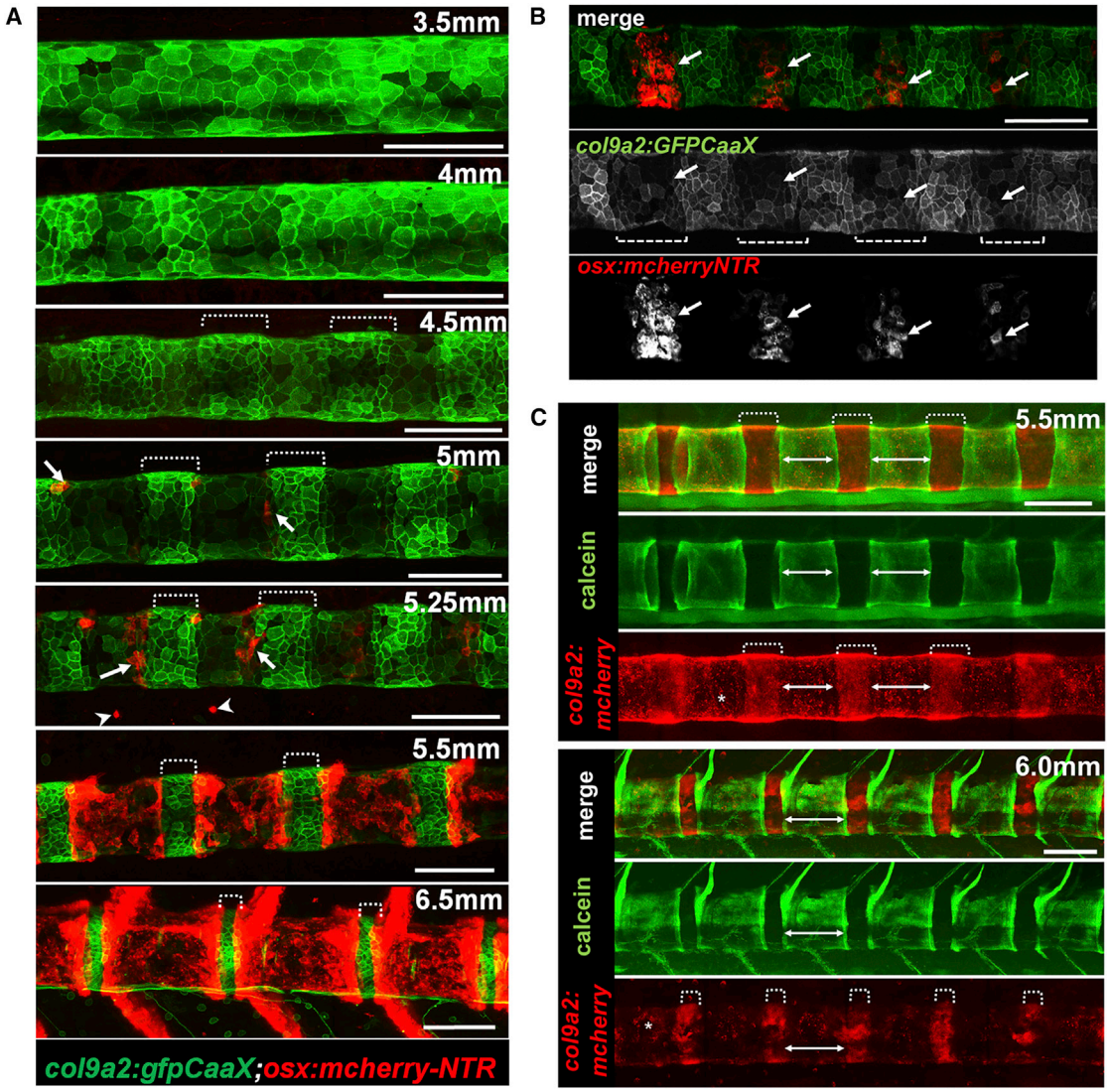

Figure 1. The Notochord Sheath Displays a Segmented Pattern Prior to Vertebral Body Formation

(A) Live confocal imaging of notochord segmentation (denoted by brackets) and osteoblast recruitment (arrows) in *col9a2:GFPCaaX* and *osx:mcherry-NTR* fish.

(B) Live confocal imaging showing that osteoblasts specifically migrate to *col9a2*-negative domains (brackets) in an anteroposterior manner.

(C) Live imaging of calcein stained *col9a2:mcherry* fish showing that *col9a2*-negative domains (denoted by asterisks) become mineralized.

Developmental stages are based on standard length. All scale bars are 100 μm. Images in (A) and (C) are digitally stitched.

and pharmacological and notochord-specific genetic manipulations indicate that the Notch pathway controls the segmentation of the notochord sheath that guides the patterning of the spine. Our work reveals a central role for the notochord in morphogenesis of the segmented spine in zebrafish.

RESULTS

The Notochord Sheath Segments into Alternating Domains Prior to Vertebral Body Formation

The zebrafish notochord consists of a core of large vacuolated cells surrounded by an epithelial sheath that secretes a thick extracellular matrix (Ellis et al., 2013b; Yamamoto et al., 2010). These notochord sheath cells have also been referred to as notochord epithelial cells or chordoblasts in the past. Vacuole inflation and integrity contribute to embryonic axis elongation and straight spine axis formation by providing a hydrostatic scaffold (Ellis et al., 2013a; Navis and Bagnat, 2015). The notochord sheath is key for scaffold formation and is essential for repairing the notochord after mechanical damage (Garcia et al., 2017; Gray et al., 2014). Previously, we generated *col9a2* zebrafish transgenic reporters that specifically label notochord sheath cells (Garcia et al., 2017). At early stages in development, *col9a2:GFPCaaX* was uniformly expressed in the plasma membrane of all sheath cells (Figure 1A). However, in larvae as early as 4.0 mm standard length (SL) (Parichy et al., 2009), we

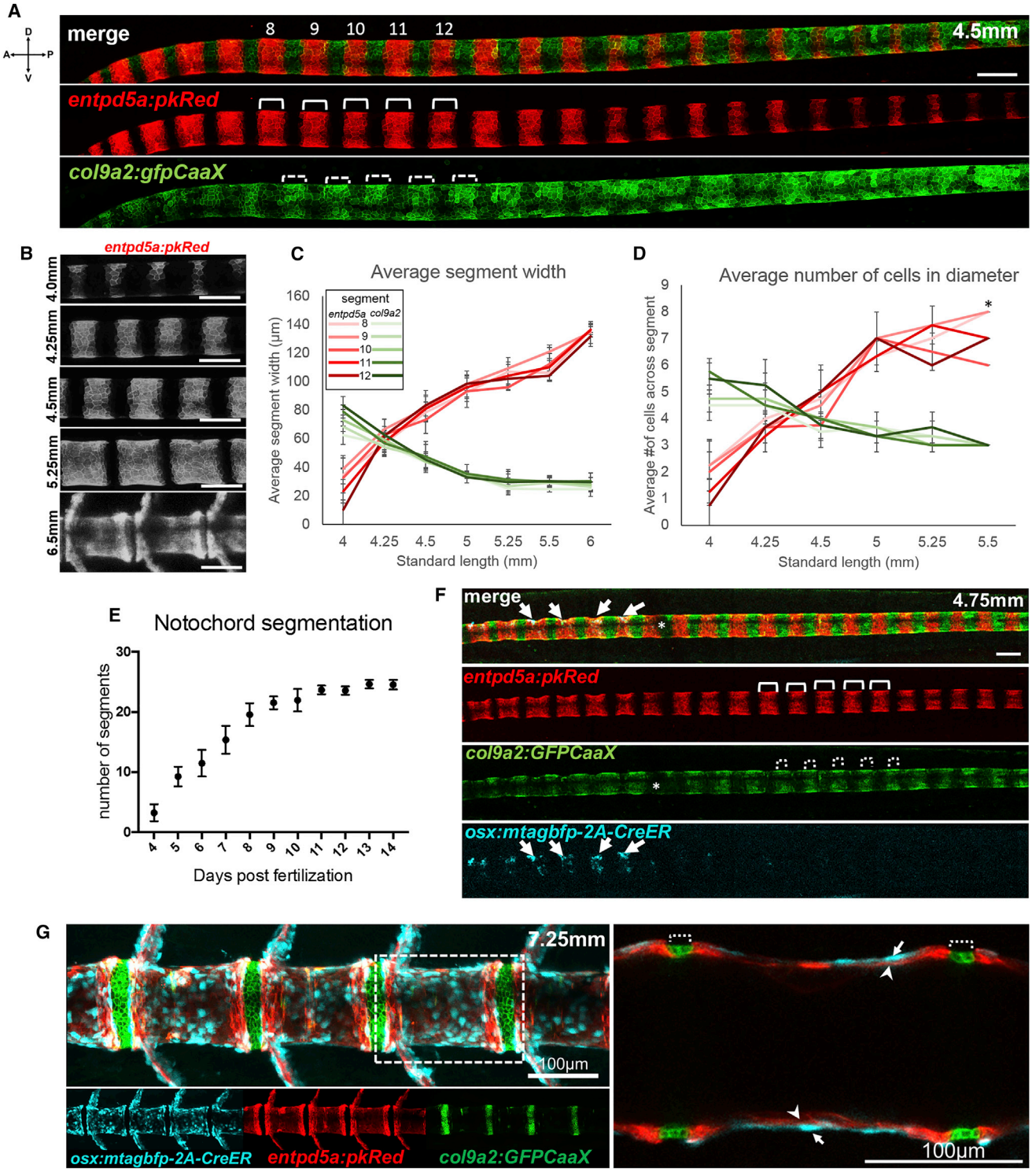

Figure 2. The Notochord Sheath Segments into Alternating Domains Prior to Spine Morphogenesis

(A) Live confocal images showing alternating *entpd5a:pkRED* (solid brackets) and *col9a2:GFPCaaX* segments (dotted brackets) in the notochord sheath of a 4.5 mm SL fish. Numbers represent the *entpd5a* segments used for quantifications.

(B) At 4.0 mm SL, *entpd5a:pkRED* expression produces segments that expand over time and completely mirror centra.

(C) *entpd5a*$^{+}$ segment length (red tones), monitored in segments 8–12, increases as *col9a2*$^{+}$ domain (green tones) length decreases in three individual fish.

(legend continued on next page)

observed a segmented pattern of *col9a2*-driven *GFPCaaX* expression that generated an alternating pattern of *col9a2*$^+$ and *col9a2*-negative domains. Temporally, this pattern emerged first in anterior regions and moved in a wave toward the posterior (Figure 1A). At late stages (6.5 mm SL), *col9a2:GFPCaax*$^+$ domains exclusively labeled the fully developed intervertebral discs (IVDs) (Figure 1A).

To understand the role of *col9a2* segmentation in spine patterning, we crossed the *col9a2* reporter to a transgenic line that labels osteoblasts, *Tg*(*osx:mcherry-NTR*) (Singh et al., 2012). Interestingly, we observed that osteoblasts were specifically recruited from the PM to patches of *col9a2*-negative regions in an anteroposterior fashion, prior to the formation of mature centra (Figures 1A and 1B). Previous work has shown that before the appearance of ossified centra, mineralized rings, called chordacentra, are formed around the zebrafish notochord sheath (Fleming et al., 2015). To visualize *col9a2* segmentation in relation to the chordacentra, we stained 5.5 mm and 6.0 mm SL *col9a2:mcherry* fish with calcein, which labels calcified structures. This clearly showed that *col9a2* expression was specific for non-mineralized segments of the notochord (Figure 1C).

Mineralized Sheath Domains Form Sequentially and Recruit Osteoblasts to Form Centra

Because notochord sheath mineralization has been shown to require ectonucleoside triphosphate/diphosphohydrolase, Entpd5a (Huitema et al., 2012), and chordacentra are likely made by the notochord sheath (Fleming et al., 2004; Grotmol et al., 2006), we used *TgBAC(entpd5a:pkRED)* animals to visualize the *col9a2*-negative notochord sheath segments. Similar to the downregulation of the *col9a2* reporter, segmented expression of *entpd5a* proceeded in an anteroposterior direction starting at about 4 days post-fertilization (dpf), or approximately 3.5 mm SL (Figures 2A and S1). Newly formed *entpd5a*$^+$ segments typically manifested as one-cell-wide vertical stripes of cells overlapping the *col9a2*$^+$ domain. Over the course of domain segregation, *entpd5a*$^+$ segments expanded at the expense of the *col9a2* domain, while cells at the border of the two domains retained expression of both transgenes (Figures 2B–2D). Because of perdurance of GFPCaaX, segmented expression of *entpd5a:pkRED* appeared to precede *col9a2* downregulation. These observations indicate that alternating notochord segments arise from a seemingly homogeneous cell population, initially labeled by uniform expression of *col9a2:GFPCaaX*. Then, cells fated to form chordacentra transition to expressing both transgenes before exclusively expressing *entpd5a:pkRED*. Tracking the appearance of new *entpd5a*$^+$ segments over time revealed that these segments were formed sequentially, approximately every 8 hr during the initial linear phase ($r^2 = 0.95$), in a manner reminiscent of somite segmentation (Figure 2E). We then imaged notochord segmentation together with the osteoblast reporter *Tg(osx:mTagBFP-2A-CreER)* (Singh et al., 2012). We observed that the alternating domains of the notochord sheath were established prior to centra formation and that osteoblasts were specifically recruited to the *entpd5a:pkRED*$^+$ domains (Figure 2F). At later stages (7.25 mm SL), we observed that osteoblasts associated with the centra completely overlaid the *entpd5a*$^+$ domains, while *col9a2:GFPCaaX* labeled the mature IVDs that were devoid of osteoblasts (Figure 2G). Taken together, these data indicate that notochord sheath cells undergo dynamic changes to generate alternating segments, one of which possesses the capacity to mineralize and recruit osteoblasts to form centra.

Transition of Cartilage-like to Mineralizing Domains Involves the Activation of Notch in the Notochord Sheath

To identify transcriptional programs underlying notochord segmentation and spine patterning, we used fluorescence-activated cell sorting (FACS) to isolate from 13 dpf larvae sheath cell populations unique to the *col9a2*$^+$ domain, the *entpd5a*$^+$ domain, or the transitional (*col9a2*$^+$/*entpd5a*$^+$ double-positive) cells. These double-positive cells include cells from both new segments and overlapping domain boundaries from older segments (Figure 3A). Isolated cell populations were then used to generate transcriptomes for each domain (Figure 3A). Principal-component and differential expression analyses confirmed that each population had unique enrichment signatures (Figures 3B and S2A). Profiling using Gene Ontology (GO) terms and Kyoto Encyclopedia of Genes and Genomes (KEGG) pathway analysis revealed that genes in the *col9a2*$^+$ domain were associated with cartilage development (e.g., *sox9b*, *col2a1*, and *matn4)* (Figures 3C and 3D; Tables S1 and S2). The transitional (*col9a2*$^+$/*entpd5a*$^+$ double-positive) domain was enriched for Notch target genes known to function in somite segmentation, such as *mespbb*, *notch1a*, and *ripply1* (Figures 3C, 3D, and S2B), and also expressed low levels of *her1*. By contrast, the *entpd5a*$^+$ domain was enriched in genes implicated in tissue mineralization and osteoblast differentiation, including *scpp1*, *sp7*, and *runx2b* (Figures 3C and 3D; Tables S1 and S2). To validate our findings and interrogate the dynamics of sheath segmentation, we generated a transgenic line to label the transitional population by isolating a promoter sequence from *id2a*, a known regulator of

(D) The number of cells within *entpd5a*$^+$ segments increase via the transition of adjacent *col9a2*$^+$ cells were measured in three individual fish. *Cells could not be counted accurately because of crowding.

(E) Monitoring the appearance of *entpd5a*$^+$ segments over time indicates new segments form sequentially every 8 hr. Between 15 and 32 fish were quantified for each time point. Means and SDs are displayed for each time point.

(F) Confocal image of a 4.75 mm SL fish showing that segregation of alternating *entpd5a*$^+$ (solid brackets) and *col9a2*$^+$ (dotted brackets) segments in the notochord sheath precedes osteoblast recruitment (cyan; marked by *osx*), which are observed only in the oldest, most anterior segments (denoted by arrows).

(G) Confocal image of a 7.25 mm SL fish showing that *entpd5a:pkRED* expression (arrowheads) underlies osteoblasts, marked by *Tg(osx:mTagBFP-2A-CreER)* expression, in the spine centra (arrows), while *col9a2:GFPCaaX* expression is confined to the IVD (dotted brackets). Right: a zoomed-in z-slice of dotted box in left image.

Developmental stages are based on standard length. Scale bars are 100 μm. Asterisk denotes interference in optical path. Images in (A), (B), and (F) are digitally stitched.

See also Figure S1.

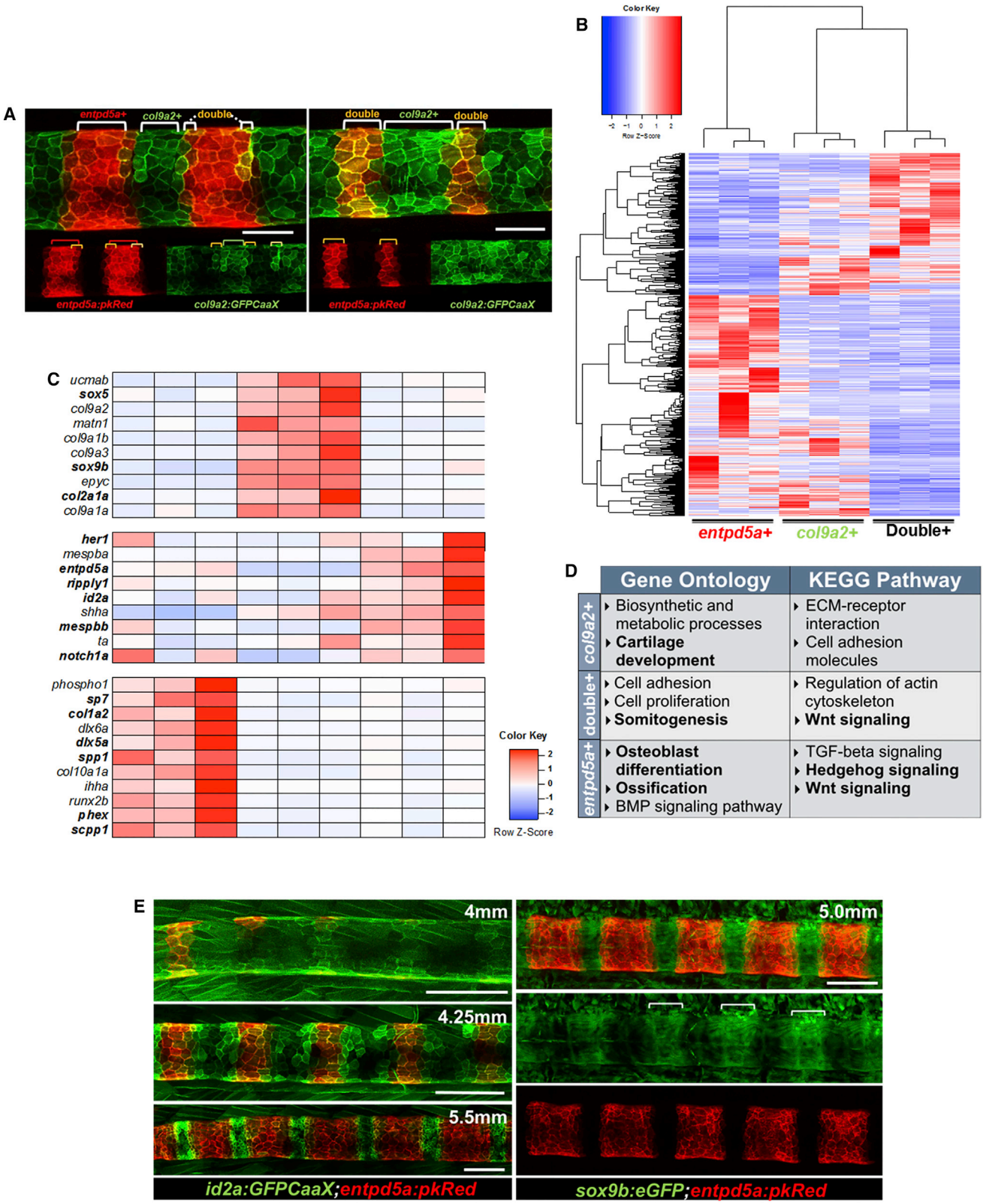

(legend on next page)

proliferation and differentiation (Uribe et al., 2012). Early in development (4.0 mm SL), *id2a:GFPCaax* exhibited a segmented pattern of expression labeling cells that later gave rise to new *entpd5a*$^+$ segments (Figure 3E). Then, as the new *entpd5a*$^+$ segments expanded (4.25 mm SL), *id2a:GFPCaaX* expression was restricted to the cells at the boundary between *col9a2*$^+$ and *entpd5a*$^+$ sheath domains. These observations are consistent with the dynamics of *entpd5a*$^+$ and *col9a2*$^+$ domains and the distinct transcriptional profile we found for the double-positive cells. Additionally, we found that *sox9b:eGFP* (Plavicki et al., 2014), a known transcriptional regulator of cartilage development (Yan et al., 2005), was enriched in the *col9a2*$^+$ domain, further supporting our transcriptomic analyses (Figure 3E). These data reveal the existence of well-defined alternating domains of gene expression in the notochord sheath corresponding to cartilage-like and mineralizing domains.

One of the most highly upregulated genes in the transitional population with respect to the *entpd5a*$^+$ and *col9a2*$^+$ populations was *mespbb*, a known target of Notch signaling (Cutty et al., 2012; Sawada et al., 2000). During zebrafish embryogenesis, *mespbb* is expressed at the determination front (somite S-I), and as segmentation proceeds its expression keeps shifting posteriorly to remain always at the anterior end of the PSM (Cutty et al., 2012; Sawada et al., 2000). In contrast, during notochord segmentation, *mespbb* expression was clearly detected in newly formed and mature segments at similar levels (Figure S3), suggesting that its expression does not oscillate in the notochord, as it does during PSM segmentation. We also attempted to image the expression of *her1:her1-venus* during notochord segmentation. Expression of this reporter has been shown to oscillate during somitogenesis (Delaune et al., 2012). However, expression levels were too low for live imaging, and we could not determine whether this gene oscillates in the notochord or not.

The transition from cartilage-like to mineralizing domains is associated with the expression of Notch target genes and mutations in Notch pathway genes have been linked to vertebral patterning defects in mouse and humans (Sparrow et al., 2012; Turnpenny et al., 2007). Therefore, we tested whether activation of Notch signaling occurs during notochord segmentation. To this end, we examined the expression pattern of a previously validated reporter of Notch activity that consists of a short-half-life form of the fluorescent protein Venus (*VenusPEST*) under the control of a Notch-responsive element (*TP1*) (Ninov et al., 2012). Interestingly, robust Notch activation could be detected in the sheath, completely overlapping with *entpd5a*$^+$ expression domains, including newly forming and mature segments (Figures 4A and 4B).

Next, we tested the effect of Notch inhibition on sheath segmentation. We found that incubation of 7 dpf larvae with the γ-secretase inhibitor DAPT for 24 hr blocked *entpd5a* induction in the sheath, whereas in larvae that were treated with DMSO, two or three new segments were formed during the same period of time (Figure 4C). Remarkably, once DAPT was washed out, *entpd5a* expression completely recovered in the segments that had been stalled (Figure 4C). To better understand the dynamics of Notch activation in the notochord, we photobleached single *TP1:VenusPEST* segments and assayed for recovery of reporter expression. We observed partial recovery of the Notch reporter expression after just 4 hr (Figure 4D) and full recovery by 24 hr in the presence of DMSO, but not when DAPT was added following photobleaching (Figure 4E). Thus, the strong signal of the Notch reporter within *entpd5a*$^+$ notochord sheath segments was due to continuous activation of Notch and not to perdurance of Venus-PEST.

Together, these data reveal that the transition from cartilage-like to mineralizing domains in the notochord sheath depends on the activation of Notch signaling at regular intervals. These data also indicate that Notch activation and sheath segmentation are not strictly linear.

Altered Notochord Sheath Segmentation Leads to Matching Segmentation Defects in the Spine

Our gene expression analyses, Notch signaling reporter, and DAPT inhibition data revealed that a Notch-dependent mechanism controls segmentation of the notochord sheath. However, DAPT inhibits Notch signaling globally and cannot be sustained for long enough to allow analysis of its effect on spine patterning. Therefore, to test whether notochord and spine segmentation could be altered by manipulating Notch signaling specifically in notochord sheath cells, we used the QF2/QUAS system (Subedi et al., 2014; Potter et al., 2010) to drive effector genes in this tissue. This experimental approach also allowed us to avoid somitogenesis defects (Figures S4A and S4B). Expression of GFP, or the system components QF2 or QUAS alone, did not lead to defects in either notochord or vertebral segmentation (Figures 5A and S4C). In contrast, constitutive activation of Notch signaling in the *col9a2* domain by expression of *notch1a* intracellular domain (*nlsVenus-V2a-notch1a*) (Eom et al., 2015) produced ectopic and indistinct patches of *entpd5a:pkRED* at 14 dpf, as

Figure 3. The Notochord Sheath Segments into Cartilage-like and Mineralizing Domains of Gene Expression

(A) Notochord sheath cells expressing *col9a2:GFPCaaX* and *entpd5a:pkRED* produce three cell populations: *col9a2*$^+$ (green bracket), double-positive (yellow bracket), and *entpd5a*$^+$ at 13 dpf or approximately 4.25 mm SL. In the same fish, mature or anterior segments express double-positive cells at borders between domains. New, more posterior segments consist of double-positive cells. Scale bar is 50 μm.

(B) Heatmap of differentially expressed genes (DEG) using scaled counts shows that the three cell populations possess distinctive clusters of upregulated genes. The color gradient indicates measures of SDs from the mean expression level of each gene.

(C) Heatmap visualization of genes within functionally annotated *col9a2*$^+$, double-positive, and *entpd5a*$^+$ populations show enrichment in genes linked to cartilage development, somite segmentation, and mineralization, respectively.

(D) Lists of top GO terms and KEGG pathways.

(E) Confocal imaging of transgenic reporter *id2a:GFPCaaX* shows dynamic expression in the notochord sheath specific to the double-positive domain. Imaging of *sox9b:eGFP* shows that expression in the notochord sheath is specific to the *col9a2*$^+$ domain.

Developmental stages are based on standard length. Scale bars are 100 μm. Images in (A) and (E) are digitally stitched. See also Figures S2 and S3 and Tables S1 and S2.

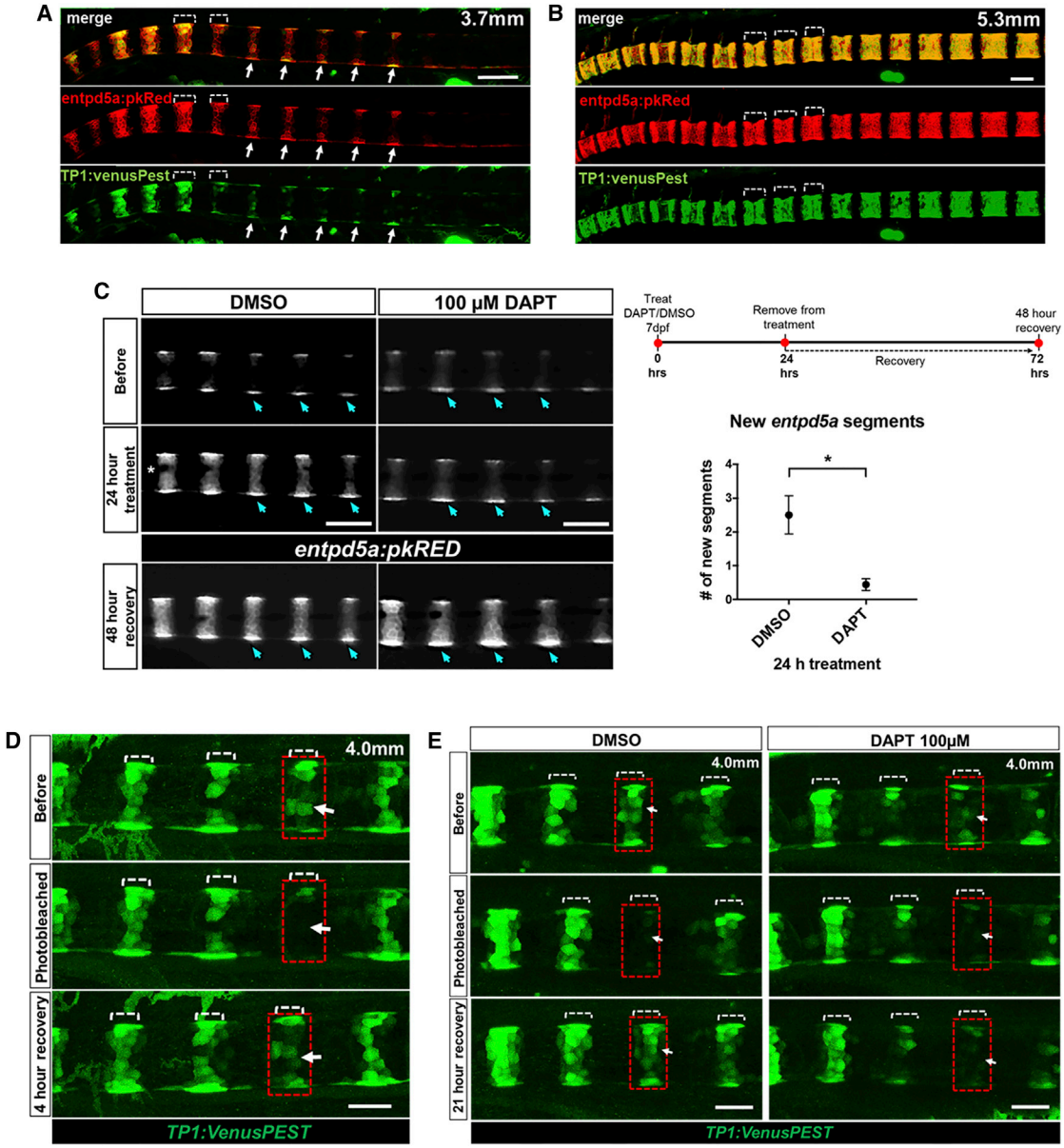

Figure 4. Activation of Notch Signaling in Alternating Sheath Domains Drives Notochord Segmentation

(A) At 3.7 mm SL, expression of *entpd5a:pkRED* and *TP1:VenusPest*, a reporter for Notch activation, shows that Notch signaling is active in double-positive and *entpd5a*$^{+}$ domains during the formation of new segments (arrows).

(B) At 5.3 mm SL, expression of *TP1:VenusPest* persists in mature *entpd5a*$^{+}$ segments.

(C) Formation of new *entpd5a*$^{+}$ segments is halted upon treatment with 100 µM DAPT in 7 dpf larvae (DAPT treated, n = 9; DMSO treated, n = 6; p = 0.013) for 24 hr (see schematic; red dots indicate imaging time point). Control embryos treated with DMSO still form two or three segments (graph). Forty-eight hours following the washout of DAPT, *entpd5a*$^{+}$ segment formation is recovered (arrows) in DAPT-treated fish. Scale bars for (A)–(C) are 100 µm.

(D) Photobleaching of a single *TP1*$^{+}$ segment (red box) in a 4.0 mm larva shows that *TP1* expression is significantly recovered by 4 hr (arrow).

(E) Recovery of the photobleached *TP1*$^{+}$ segment (red box) is complete by 21 hr in DMSO but not in 100 µM DAPT. Scale bars for (D) and (E) are 50 µm.

opposed to well-defined segmented domains (Figure 5B). At later stages, these early defects resolved into wedge, short, and pebble vertebrae, as visualized by staining with alizarin red (Figures 5B and S5A). These more severe phenotypes are strikingly similar to the pebble vertebrae observed in humans with mutations in Notch pathway genes (Turnpenny et al., 2007). When Notch signaling was inhibited in the *col9a2* domain by targeted expression of a dominant-negative suppressor of hairless (*nVenus-V2a-SuHDN*) cassette (Eom et al., 2015), we observed that *entpd5a*$^{+}$ sheath segments were missing or only partially

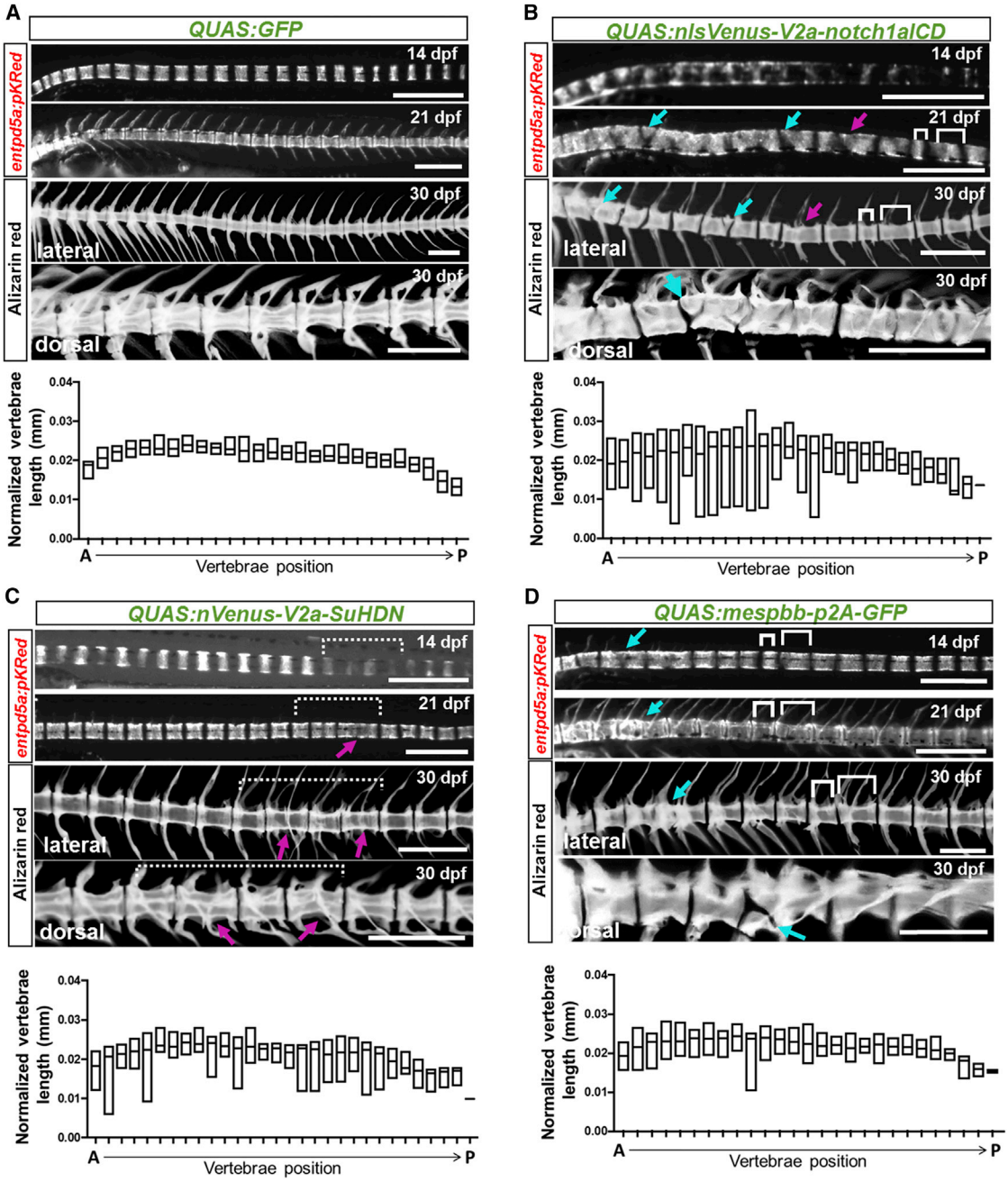

Figure 5. Alteration of Notochord Sheath Segmentation Produces Matching Defects in Spine Segmentation

(A) Bright-field imaging of *entpd5a:pkRED* expression in the notochord sheath using the QF2/QUAS system to overexpress GFP does not alter segmentation. Vertebrae length measurements in 30 dpf fish were normalized to standard length (n = 19).

(B) Constitutive activation of Notch signaling via expression of *QUAS:nlsVenus-V2a-notch1alCD* within the notochord sheath generates patchy *entpd5a:pkRED* segments at 14 dpf. At 21 dpf, some mature notochord segments are wedged, incomplete (cyan arrows), or irregularly sized (magenta arrows). Alizarin red staining revealed the same defects in the spine. Quantification of vertebra length normalized to the standard length showed highly variable size, particularly in the anterior portion of the spine, significantly deviating from the GFP control (n = 20, p = 0.0001).

(C) Inhibition of Notch signaling via expression of *QUAS:nVenus-V2a-SuHDN* resulted in partial or skipped *entpd5a:pkRED* segments producing gaps in the posterior region of the notochord at 14 dpf (dotted bracket). At 21 dpf, smaller *entpd5a* segments (magenta arrows) fill in gaps. Alizarin staining shows that these defects resulted in irregular spacing and fusions of vertebrae (magenta arrows). Measurements of vertebra length normalized to standard length showed irregularly sized vertebrae, particularly in the posterior portion of the spine, but the majority of these measurements did not differ significantly from the GFP control (n = 16).

(legend continued on next page)

formed at 14 dpf (Figure 5C). This manipulation generated gaps in the *entpd5a*$^{+}$ domain that were filled later by more but smaller and fused *entpd5a*$^{+}$ segments at the posterior end of the notochord and spine (Figures 5C and S5B). Together, these data indicate that Notch signaling in notochord sheath cells controls the induction of *entpd5a*$^{+}$ domains that eventually give rise to mature centra.

In zebrafish, overexpression of *mesp* during somitogenesis has been shown to cause severe segmentation defects (Sawada et al., 2000; Windner et al., 2015), and loss of function of the *mesp* genes alters somite boundary formation (Yabe et al., 2016). Moreover, orthologs of *mespbb* in mice and humans have been shown to cause vertebral defects (Sparrow et al., 2012; Turnpenny et al., 2007). Therefore, we decided to test whether misexpression of *mespbb* in the *col9a2* domain of the sheath could alter boundary formation. Misexpression of *QUAS:mespbb-p2A-GFP* early in development caused embryonic defects. To bypass the early developmental defects, we injected QS (Potter et al., 2010) mRNA at the one-cell stage to inhibit QF2 during early development (Figure S6). Under these conditions, the onset of *QUAS:mespbb-p2A-GFP* misexpression was delayed, allowing the development of notochord segments and spine centra that showed variable lengths throughout the axis (Figure 5D). On average, centra were longer and their number was decreased in fish expressing *QUAS:mespbb-p2A-eGFP* compared with controls (Figures S5B and S5C). These data suggest that expression of *mespbb* in the notochord sheath regulates segment size, possibly via regulating boundary formation and Notch, as has been shown in the mouse PM (Sasaki et al., 2011).

Together, our genetic manipulations indicate that Notch-dependent notochord sheath segmentation instructs the precise patterning of centra in the zebrafish spine.

DISCUSSION

We have found that zebrafish notochord sheath cells segment into alternating mineralizing and cartilage-like domains and that selective recruitment of osteoblasts to only one of these domains (the mineralized domains) underlies the segmented patterning of the spine. It is also possible that the *col9a2*$^{+}$ domains somehow repel osteoblasts as well, thereby contributing to the specification of the IVD. Our work reveals that the establishment of the instructive pattern of the sheath involves the activation of Notch signaling in alternating domains of notochord sheath cells.

Several features of the notochord sheath segmentation process shown here are generally reminiscent of the somite segmentation clock, suggesting that a similar mechanism acts in the notochord. However, several lines of evidence argue against a clock-like mechanism controlling notochord sheath segmentation. First, in contrast to what has been shown for somitogenesis, Notch signaling is continuously active and seemingly uniform in all the mineralizing notochord sheath segments (Figure 4). Second, *mespbb* expression does not seem to oscillate in the notochord, as it does in the PSM (Figure S3). Third, the generation of segments is not strictly linear in time and direction in the notochord sheath, as is the case of somitogenesis. That is, notochord segments can recover and be filled in following transient inhibition (Figure 4C). In contrast, areas of the PSM that are affected by Notch inhibition (e.g., transient DAPT treatment) do not recover (Ozbudak and Lewis, 2008). Fourth, the notochord is still segmented in areas adjacent to unsegmented PM (Figures 6A and 6B). Although it cannot be formally excluded that a form of the segmentation clock acts in the notochord, such clock would have to be differentially regulated in the sheath with respect to the PM. Indeed, genetic impairment of segmentation clock genes *her1*, *her7*, *hes6*, and *tbx6* leaves notochord sheath segmentation largely intact (L. Lleras-Forero and S.S.-M., unpublished data). Another important difference is that the notochord sheath segments into two distinct domains of epithelial cells rather than into identical units of mesenchyme separated by epithelial boundaries. The absence of a topological transition such as the one that occurs during somitogenesis may explain the need for continuous activation of Notch signaling to maintain domain segregation in the segmented notochord sheath.

Our work suggests that in addition to differentiation of distinct cell populations, continuous Notch activation is also required for sheath mineralization, at least in part through the control of *entpd5a* expression. Notch signaling has been implicated in mineralization in other contexts (Liu et al., 2016), and it is a common theme in a wide range of differentiation processes such the one shown here. However, it is unclear whether mineralization and differentiation are separable processes in the notochord. Future work with more precise genetic tools will be needed to explore this question further.

How Notch signaling is initiated in space and time and how it spreads laterally to produce segments of precise length and sharp boundaries remain unclear. It is possible that Notch-dependent mechanisms such as stripe refinement (Corson et al., 2017) and lateral induction (Saravanamuthu et al., 2009) regulate segment expansion and boundary formation. The control of segment size is likely influenced by the spacing of segments, as irregularly spaced sheath segments are also unevenly sized (Figures 6A–6D). Our data also suggest that notochord and spine segment size and number are linked (e.g., misexpression of *mespbb* produces less segments that are also larger; Figures S5B and S5C). Regulation of notochord segment size and boundaries may involve negative feedback loops regulated by

(D) Misexpression of *mespbb* generates partial (cyan arrow) and variably sized segments (brackets) at 14 dpf. The same defects were observed at 21 and 30 dpf in the mature spine at the same positions. Vertebrae length measurements showed high variability throughout the spine axis, significantly different from the GFP control ($n = 22$, $p = 0.0104$). Onset and level of *mespbb* misexpression were attenuated by injection of QS mRNA.

Scale bars are 500 μm. Vertebrae position started with the first rib-bearing vertebra to the last caudal vertebra. We did not include the Weberian apparatus or the tail vertebrae in our analysis. The p values for vertebrae length comparisons were calculated from a one-way ANOVA with Dunnett's multiple-comparisons test. Skeletal preps were converted to black-and-white images and inverted to better highlight defects. Floating bars in graphs display the minimum and maximum range for normalized vertebrae length (mm). Lines denote median values.

See also Figures S4–S6.

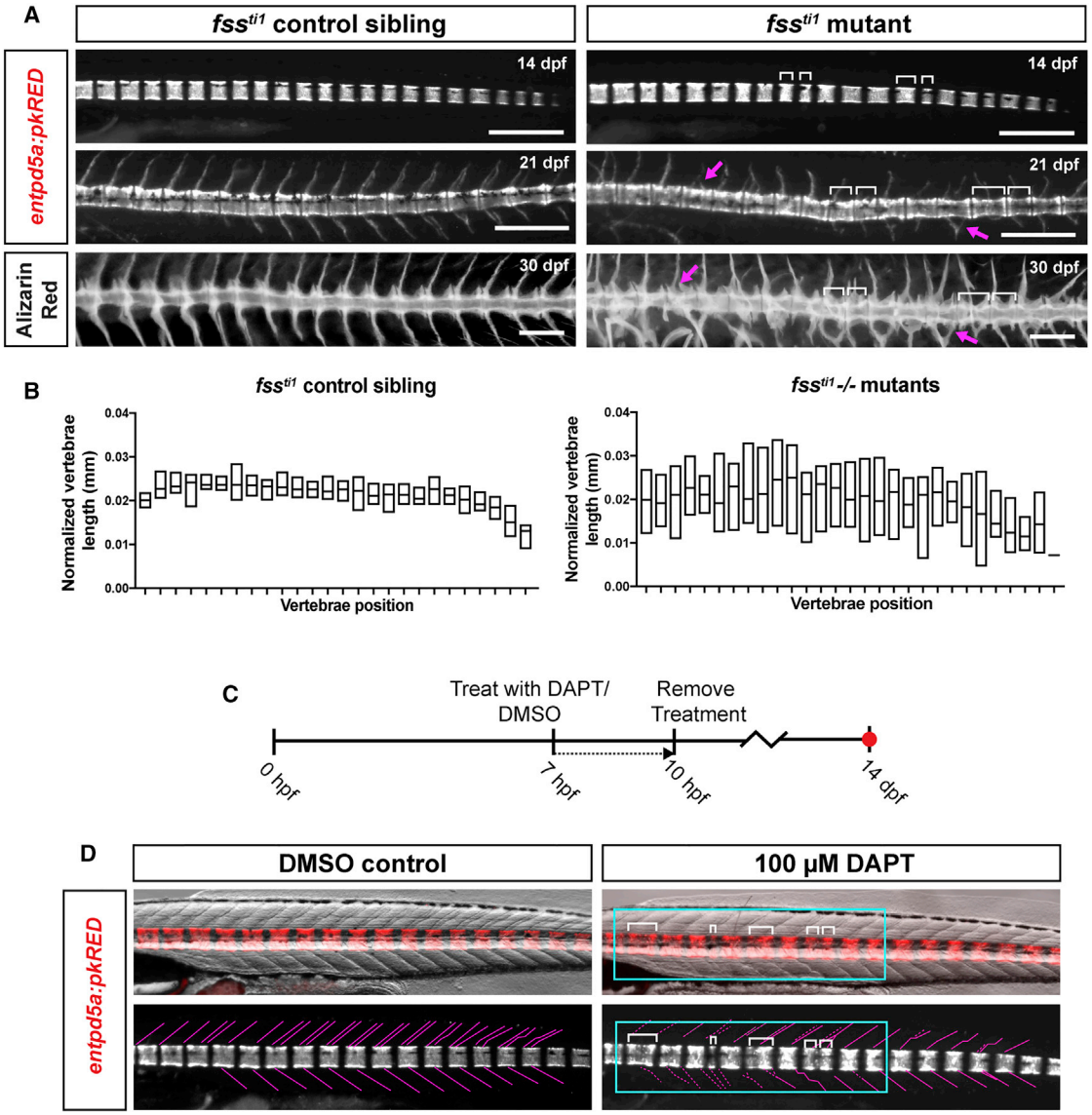

Figure 6. Somite Boundaries Influence the Spatial Distribution of Notochord Sheath Segments

(A) Bright-field imaging of *entpd5a:pkRED* at 14 dpf *tbx6* mutants (*fss*^{ti1}) shows that notochord segments (brackets) exhibit high size variability compared with their wild-type (WT) siblings. Following the same fish at 21 dpf, the same pattern was also observed. At 30 dpf, alizarin red stains show that mutants develop severely deformed arches (magenta arrows) and variably sized centra.

(B) Quantification of centra length in calcein stained *tbx6* mutants (*fss*^{ti1}) at 21 dpf showed greater variability compared with WT siblings (n = 14 and 11 for mutant and WT, respectively, $p \leq 0.0001$).

(C) Embryos were exposed to 100 μM DAPT or DMSO treatment at 7 hr post-fertilization (hpf) for 3 hr (red dot indicates imaging time point).

(D) Embryos exposed to 100 μM DAPT develop focal defects in somite segmentation (cyan box outlines disrupted somite boundaries traced with dotted pink lines). Bright-field imaging of 14 dpf *entpd5a:pkRED* showed defects in notochord segment size and spacing (brackets) after DAPT was washed out compared with control DMSO-treated animals.

Scale bars are 500 μm.

effectors such as *mespbb* and *id2a* (Uribe et al., 2012; Windner et al., 2015; Yabe and Takada, 2016).

On the other hand, the location and spacing of new notochord segments seem to be influenced by interactions between the notochord and the PM. In null mutants for *tbx6* (also known as *fss*^{ti1}), somite boundaries are lost or disorganized (Brend and Holley, 2009; van Eeden et al., 1996), and notochord and vertebral segments show a high level of variance in length that can be traced to the irregular placement of new *entpd5a*$^{+}$ segments (Figures 6A and 6B). Interestingly, a similar phenotype occurs when somite boundaries are locally affected by transient exposure to DAPT during somitogenesis (Figures 6C and 6D),

suggesting that somite boundaries somehow contribute to the precise placement of adjacent *entpd5a*$^{+}$ notochord segments. The rostro-caudal polarization of somites may serve as a mechanism to allocate the sclerotome populations that migrate toward the mineralized domains of the notochord sheath along somite boundaries to form each centrum.

Our study fills an important gap in our understanding of spine patterning. However, many questions remain open and new ones have emerged. Uncovering the cellular and molecular mechanisms controlling the precise activation and spreading of Notch signaling domains during notochord segmentation is key for elucidating the origin of vertebral defects.

EXPERIMENTAL PROCEDURES

Further details and an outline of resources used in this work can be found in Supplemental Experimental Procedures.

Notochord Sheath Cell Isolation for RNA Sequencing

Notochords from Tg(*col9a2:GFPCaaX;entpd5a:pkRED*) fish were dissociated to generate single-cell suspensions for FACS by incubating in 0.25% trypsin-EDTA (GIBCO) and 1% collagenase (Sigma-Aldrich) at 32°C for approximately 1 hr. Dissociations were encouraged by pipetting every 5–10 min. Propidium iodide (Invitrogen) was added to the sample before FACS to filter out dead cells. Total RNA was prepared from each population using RNeasy Plus Micro Kit (QIAGEN). RNA samples were evaluated for concentration by Qubit (Thermo Fisher Scientific) and for integrity using an Agilent 2100 Bioanalyzer. Samples with an RNA integrity number (RIN) >7.0 were used for RNA sequencing (RNA-seq) analysis. Clontech Ultra low libraries were prepared in triplicate and sequenced using the Illumina HiSeq 4000 50 bp single-end read platform. Sequencing data were uploaded to the Galaxy Web platform, and we used the public server at https://usegalaxy.org for analysis (Afgan et al., 2016). Reads were mapped to the GRCz10 (danRer10) genome using HISAT2, and gene counts were analyzed using htseq-counts (Kim et al., 2015). htseq-counts were input into DESeq2 to calculate differential expression for cell populations (Anders et al., 2015; Love et al., 2014). Genes were considered to be enriched in a population if their expression was at least 2-fold greater in comparison with the other population with an adjusted p value of <0.05. Principal-component analysis was performed in R using the DESeq2 package. All KEGG pathway and GO term analysis was performed using DAVID Bioinformatics Resources 6.8 (Huang et al., 2009a, 2009b). Heatmaps were generated using the gplots package in R.

Microscopy

Whole-mount confocal live imaging was performed on a Fluoview FV3000 (Olympus) confocal microscope equipped with 30×/1.05 silicone oil objective (Olympus) and Fluoview software (Olympus) and an SP5 upright confocal microscope (Leica) equipped with a 20×/0.70 HC PL APO oil objective (Leica) and Application Suite software (Leica). Fish were mounted onto glass-bottom dishes in a 1.5% agarose mixture of egg water and 1× tricaine or using slides with 3% methylcellulose and 1× tricaine, encircled in a ring of vacuum grease. Additional imaging was done using a AX10 Zoom V116 Zeiss microscope equipped with a Plan neofluar Z 1× objective and Zen software (all from Carl Zeiss). When necessary, images were minimally processed in ImageJ software (NIH) for brightness and contrast. Digital stitching of confocal images (Figures 1A, 1C, 2A, 2B, 2F, 3A, and 3E) was done in Fluoview software.

For photobleaching, *TP1:VenusPEST* transgenic fish were mounted onto glass-bottom dishes in 3% methylcellulose and 1× tricaine and imaged using the Fluoview FV3000 with 30×/1.05 silicone oil objective (Olympus). Prior to photobleaching, an initial image was taken. Using LSM stimulation in Fluoview software, laser scanning was specifically targeted to one segment, which was bleached after three scans at 80% laser power lasting 30 s each. Fish were rescued in egg water and left to recover at 28°C in egg water, 100 μM DAPT, or DMSO control.

Statistical Analyses

GraphPad Prism version 7.0c for Mac (GraphPad Software) and Microsoft Excel were used to analyze and plot data. Microsoft Excel was used to plot and calculate SDs for segment length and segment cell number for Figures 2C and 2D, respectively. For Figures 4C and 5A–5D, n represents the number of individual fish analyzed. Statistical analysis for vertebrae length comparisons were calculated from a one-way ANOVA with Dunnett's multiple-comparisons test in GraphPad Prism.

Experimental Model and Subject Details

Animal experiments were approved by the Duke Institutional Animal Care and Use Committee (IACUC).

DATA AND SOFTWARE AVAILABILITY

The accession number for the raw and processed RNA-seq data reported in this paper is GEO: GSE109176.

SUPPLEMENTAL INFORMATION

Supplemental Information includes Supplemental Experimental Procedures, six figures, and two tables and can be found with this article online at https://doi.org/10.1016/j.celrep.2018.01.084.

ACKNOWLEDGMENTS

We thank Brigid Hogan, Terry Lechler, Cagla Eroglu, Blanche Capel, E.M. De Robertis, and the Bagnat lab for discussions and critical reading of the manuscript. We would like to thank Colin Likwar for help with RNA-seq analyses and Ted Espenschied for help with statistical analyses. We also thank M. Halpern, C.J. Potter, S. Amacher, S. Seyfried, S.J. Cutty, D. Parichy, W. Heideman, K. Kawakami, N. Ninov, and D.Y.R. Stainier for zebrafish lines and plasmids. This work was supported by NIH grants R01 AR065439-04 (M.B.) and R01 GM074057 (K.D.P.). The research of M.B. was supported in part by a Faculty Scholar grant, HHMI 55108501, from the Howard Hughes Medical Institute. Work by S.S.-M. was supported by the CiM Cluster of Excellence (WWU Münster, Germany) EXC 1003-CiM.

AUTHOR CONTRIBUTIONS

Conceptualization, M.B.; Methodology, M.B., S.W., J.B., K.D.S., and A.L.D.; Validation, S.W., J.B., and K.D.S.; Formal Analysis, M.B., S.W., and K.D.S.; Investigation, S.W., J.B., K.D.S., A.L.D., and M.B.; Resources, M.B., S.W., J.B., L.F.H, K.D.P., and S.S.-M.; Writing – Original Draft, S.W. and M.B.; Writing – Review & Editing, M.B., S.W., J.B., S.S.-M., and K.D.P; Visualization, J.B., S.W., and M.B.; Supervision, M.B.; Project Administration, M.B. and J.B.; Funding Acquisition, M.B.

DECLARATION OF INTERESTS

The authors declare no competing interests.

Received: October 7, 2017
Revised: January 10, 2018
Accepted: January 26, 2018
Published: February 20, 2018

REFERENCES

Afgan, E., Baker, D., van den Beek, M., Blankenberg, D., Bouvier, D., Čech, M., Chilton, J., Clements, D., Coraor, N., Eberhard, C., et al. (2016). The Galaxy platform for accessible, reproducible and collaborative biomedical analyses: 2016 update. Nucleic Acids Res. *44* (*W1*), W3–W10.

Anders, S., Pyl, P.T., and Huber, W. (2015). HTSeq—a Python framework to work with high-throughput sequencing data. Bioinformatics *31*, 166–169.

Bagnall, K.M., Higgins, S.J., and Sanders, E.J. (1988). The contribution made by a single somite to the vertebral column: experimental evidence in support of resegmentation using the chick-quail chimaera model. Development *103*, 69–85.

Brend, T., and Holley, S.A. (2009). Expression of the oscillating gene her1 is directly regulated by Hairy/Enhancer of Split, T-box, and Suppressor of Hairless proteins in the zebrafish segmentation clock. Dev. Dyn. *238*, 2745–2759.

Choi, K.S., and Harfe, B.D. (2011). Hedgehog signaling is required for formation of the notochord sheath and patterning of nuclei pulposi within the intervertebral discs. Proc. Natl. Acad. Sci. U S A *108*, 9484–9489.

Corson, F., Couturier, L., Rouault, H., Mazouni, K., and Schweisguth, F. (2017). Self-organized Notch dynamics generate stereotyped sensory organ patterns in *Drosophila*. Science *356*, eaai7407.

Cutty, S.J., Fior, R., Henriques, P.M., Saúde, L., and Wardle, F.C. (2012). Identification and expression analysis of two novel members of the Mesp family in zebrafish. Int. J. Dev. Biol. *56*, 285–294.

Delaune, E.A., François, P., Shih, N.P., and Amacher, S.L. (2012). Single-cell-resolution imaging of the impact of Notch signaling and mitosis on segmentation clock dynamics. Dev. Cell *23*, 995–1005.

Ellis, K., Bagwell, J., and Bagnat, M. (2013a). Notochord vacuoles are lysosome-related organelles that function in axis and spine morphogenesis. J. Cell Biol. *200*, 667–679.

Ellis, K., Hoffman, B.D., and Bagnat, M. (2013b). The vacuole within: how cellular organization dictates notochord function. Bioarchitecture *3*, 64–68.

Eom, D.S., Bain, E.J., Patterson, L.B., Grout, M.E., and Parichy, D.M. (2015). Long-distance communication by specialized cellular projections during pigment pattern development and evolution. eLife *4*, 4.

Ewan, K.B., and Everett, A.W. (1992). Evidence for resegmentation in the formation of the vertebral column using the novel approach of retroviral-mediated gene transfer. Exp. Cell Res. *198*, 315–320.

Fleming, A., Keynes, R., and Tannahill, D. (2004). A central role for the notochord in vertebral patterning. Development *131*, 873–880.

Fleming, A., Kishida, M.G., Kimmel, C.B., and Keynes, R.J. (2015). Building the backbone: the development and evolution of vertebral patterning. Development *142*, 1733–1744.

Garcia, J., Bagwell, J., Njaine, B., Norman, J., Levic, D.S., Wopat, S., Miller, S.E., Liu, X., Locasale, J.W., Stainier, D.Y.R., et al. (2017). Sheath cell invasion and trans-differentiation repair mechanical damage caused by loss of caveolae in the zebrafish notochord. Curr. Biol. *27*, 1982–1989.e3.

Gray, R.S., Wilm, T.P., Smith, J., Bagnat, M., Dale, R.M., Topczewski, J., Johnson, S.L., and Solnica-Krezel, L. (2014). Loss of col8a1a function during zebrafish embryogenesis results in congenital vertebral malformations. Dev. Biol. *386*, 72–85.

Grotmol, S., Kryvi, H., Nordvik, K., and Totland, G.K. (2003). Notochord segmentation may lay down the pathway for the development of the vertebral bodies in the Atlantic salmon. Anat. Embryol. (Berl.) *207*, 263–272.

Grotmol, S., Kryvi, H., Keynes, R., Krossøy, C., Nordvik, K., and Totland, G.K. (2006). Stepwise enforcement of the notochord and its intersection with the myoseptum: an evolutionary path leading to development of the vertebra? J. Anat. *209*, 339–357.

Haga, Y., Dominique, V.J., 3rd, and Du, S.J. (2009). Analyzing notochord segmentation and intervertebral disc formation using the twhh:gfp transgenic zebrafish model. Transgenic Res. *18*, 669–683.

Holley, S.A., Jülich, D., Rauch, G.J., Geisler, R., and Nüsslein-Volhard, C. (2002). her1 and the notch pathway function within the oscillator mechanism that regulates zebrafish somitogenesis. Development *129*, 1175–1183.

Huang, W., Sherman, B.T., and Lempicki, R.A. (2009a). Bioinformatics enrichment tools: paths toward the comprehensive functional analysis of large gene lists. Nucleic Acids Res. *37*, 1–13.

Huang, W., Sherman, B.T., and Lempicki, R.A. (2009b). Systematic and integrative analysis of large gene lists using DAVID bioinformatics resources. Nat. Protoc. *4*, 44–57.

Hubaud, A., and Pourquié, O. (2014). Signalling dynamics in vertebrate segmentation. Nat. Rev. Mol. Cell Biol. *15*, 709–721.

Huitema, L.F., Apschner, A., Logister, I., Spoorendonk, K.M., Bussmann, J., Hammond, C.L., and Schulte-Merker, S. (2012). Entpd5 is essential for skeletal mineralization and regulates phosphate homeostasis in zebrafish. Proc. Natl. Acad. Sci. U S A *109*, 21372–21377.

Jiang, Y.J., Aerne, B.L., Smithers, L., Haddon, C., Ish-Horowicz, D., and Lewis, J. (2000). Notch signalling and the synchronization of the somite segmentation clock. Nature *408*, 475–479.

Kim, D., Langmead, B., and Salzberg, S.L. (2015). HISAT: a fast spliced aligner with low memory requirements. Nat. Methods *12*, 357–360.

Liao, B.K., Jörg, D.J., and Oates, A.C. (2016). Faster embryonic segmentation through elevated Delta-Notch signalling. Nat. Commun. *7*, 11861.

Liu, P., Ping, Y., Ma, M., Zhang, D., Liu, C., Zaidi, S., Gao, S., Ji, Y., Lou, F., Yu, F., et al. (2016). Anabolic actions of Notch on mature bone. Proc. Natl. Acad. Sci. U S A *113*, E2152–E2161.

Love, M.I., Huber, W., and Anders, S. (2014). Moderated estimation of fold change and dispersion for RNA-seq data with DESeq2. Genome Biol. *15*, 550.

Morin-Kensicki, E.M., Melancon, E., and Eisen, J.S. (2002). Segmental relationship between somites and vertebral column in zebrafish. Development *129*, 3851–3860.

Navis, A., and Bagnat, M. (2015). Developing pressures: fluid forces driving morphogenesis. Curr. Opin. Genet. Dev. *32*, 24–30.

Ninov, N., Borius, M., and Stainier, D.Y. (2012). Different levels of Notch signaling regulate quiescence, renewal and differentiation in pancreatic endocrine progenitors. Development *139*, 1557–1567.

Oates, A.C., Morelli, L.G., and Ares, S. (2012). Patterning embryos with oscillations: structure, function and dynamics of the vertebrate segmentation clock. Development *139*, 625–639.

Ozbudak, E.M., and Lewis, J. (2008). Notch signalling synchronizes the zebrafish segmentation clock but is not needed to create somite boundaries. PLoS Genet. *4*, e15.

Parichy, D.M., Elizondo, M.R., Mills, M.G., Gordon, T.N., and Engeszer, R.E. (2009). Normal table of postembryonic zebrafish development: staging by externally visible anatomy of the living fish. Dev. Dyn. *238*, 2975–3015.

Plavicki, J.S., Baker, T.R., Burns, F.R., Xiong, K.M., Gooding, A.J., Hofsteen, P., Peterson, R.E., and Heideman, W. (2014). Construction and characterization of a sox9b transgenic reporter line. Int. J. Dev. Biol. *58*, 693–699.

Potter, C.J., Tasic, B., Russler, E.V., Liang, L., and Luo, L. (2010). The Q system: a repressible binary system for transgene expression, lineage tracing, and mosaic analysis. Cell *141*, 536–548.

Pourquié, O. (2011). Vertebrate segmentation: from cyclic gene networks to scoliosis. Cell *145*, 650–663.

Remak, R. (1855). Untersuchungen uber die Entwickling der Wirbelthiere (Verlag von G. Reimer), pp. 40–44.

Renn, J., Büttner, A., To, T.T., Chan, S.J., and Winkler, C. (2013). A col10a1:nlGFP transgenic line displays putative osteoblast precursors at the medaka notochordal sheath prior to mineralization. Dev. Biol. *381*, 134–143.

Saravanamuthu, S.S., Gao, C.Y., and Zelenka, P.S. (2009). Notch signaling is required for lateral induction of Jagged1 during FGF-induced lens fiber differentiation. Dev. Biol. *332*, 166–176.

Sasaki, N., Kiso, M., Kitagawa, M., and Saga, Y. (2011). The repression of Notch signaling occurs via the destabilization of mastermind-like 1 by Mesp2 and is essential for somitogenesis. Development *138*, 55–64.

Sawada, A., Fritz, A., Jiang, Y.J., Yamamoto, A., Yamasu, K., Kuroiwa, A., Saga, Y., and Takeda, H. (2000). Zebrafish Mesp family genes, mesp-a and mesp-b are segmentally expressed in the presomitic mesoderm, and Mesp-b confers the anterior identity to the developing somites. Development *127*, 1691–1702.

Singh, S.P., Holdway, J.E., and Poss, K.D. (2012). Regeneration of amputated zebrafish fin rays from de novo osteoblasts. Dev. Cell *22*, 879–886.

Sparrow, D.B., Chapman, G., Smith, A.J., Mattar, M.Z., Major, J.A., O'Reilly, V.C., Saga, Y., Zackai, E.H., Dormans, J.P., Alman, B.A., et al. (2012). A mechanism for gene-environment interaction in the etiology of congenital scoliosis. Cell *149*, 295–306.

Subedi, A., Macurak, M., Gee, S.T., Monge, E., Goll, M.G., Potter, C.J., Parsons, M.J., and Halpern, M.E. (2014). Adoption of the Q transcriptional regulatory system for zebrafish transgenesis. Methods *66*, 433–440.

Turnpenny, P.D., Alman, B., Cornier, A.S., Giampietro, P.F., Offiah, A., Tassy, O., Pourquié, O., Kusumi, K., and Dunwoodie, S. (2007). Abnormal vertebral segmentation and the notch signaling pathway in man. Dev. Dyn. *236*, 1456–1474.

Uribe, R.A., Kwon, T., Marcotte, E.M., and Gross, J.M. (2012). Id2a functions to limit Notch pathway activity and thereby influence the transition from proliferation to differentiation of retinoblasts during zebrafish retinogenesis. Dev. Biol. *371*, 280–292.

van Eeden, F.J., Granato, M., Schach, U., Brand, M., Furutani-Seiki, M., Haffter, P., Hammerschmidt, M., Heisenberg, C.P., Jiang, Y.J., Kane, D.A., et al. (1996). Mutations affecting somite formation and patterning in the zebrafish, Danio rerio. Development *123*, 153–164.

Wang, S., Furmanek, T., Kryvi, H., Krossøy, C., Totland, G.K., Grotmol, S., and Wargelius, A. (2014). Transcriptome sequencing of Atlantic salmon (Salmo salar L.) notochord prior to development of the vertebrae provides clues to regulation of positional fate, chordoblast lineage and mineralisation. BMC Genomics *15*, 141.

Ward, L., Evans, S.E., and Stern, C.D. (2017). A resegmentation-shift model for vertebral patterning. J. Anat. *230*, 290–296.

Watterson, R.L., Fowler, I., and Fowler, B.J. (1954). The role of the neural tube and notochord in development of the axial skeleton of the chick. Am. J. Anat. *95*, 337–399.

Windner, S.E., Doris, R.A., Ferguson, C.M., Nelson, A.C., Valentin, G., Tan, H., Oates, A.C., Wardle, F.C., and Devoto, S.H. (2015). Tbx6, Mesp-b and Ripply1 regulate the onset of skeletal myogenesis in zebrafish. Development *142*, 1159–1168.

Yabe, T., and Takada, S. (2016). Molecular mechanism for cyclic generation of somites: lessons from mice and zebrafish. Dev. Growth Differ. *58*, 31–42.

Yabe, T., Hoshijima, K., Yamamoto, T., and Takada, S. (2016). Quadruple zebrafish mutant reveals different roles of Mesp genes in somite segmentation between mouse and zebrafish. Development *143*, 2842–2852.

Yamamoto, M., Morita, R., Mizoguchi, T., Matsuo, H., Isoda, M., Ishitani, T., Chitnis, A.B., Matsumoto, K., Crump, J.G., Hozumi, K., et al. (2010). Mib-Jag1-Notch signalling regulates patterning and structural roles of the notochord by controlling cell-fate decisions. Development *137*, 2527–2537.

Yan, Y.L., Willoughby, J., Liu, D., Crump, J.G., Wilson, C., Miller, C.T., Singer, A., Kimmel, C., Westerfield, M., and Postlethwait, J.H. (2005). A pair of Sox: distinct and overlapping functions of zebrafish sox9 co-orthologs in craniofacial and pectoral fin development. Development *132*, 1069–1083.